

# CONDENSATION HEAT TRANSFER CHARACTERISTICS OF AMTEC POROUS WICK CONDENSER

*Lan XIAO* \*, *Deng ZHANG*<sup>1</sup>, *Shuang-ying WU*<sup>2</sup>, *Hui-jia YU*<sup>3</sup>

<sup>\*1</sup> Key Laboratory of Low-grade Energy Utilization Technologies and Systems, Ministry of Education, Chongqing University, Chongqing 400044, China

<sup>2</sup> College of Power Engineering, Chongqing University, Chongqing 400044, China

<sup>3</sup> Chongqing Energy College, Chongqing 400044, China

\* Corresponding author; E-mail: xiaolannancy@cqu.edu.cn

*An axisymmetric two-dimensional mathematical model was established and the volume of fluid (VOF) method was adopted to numerically investigate the condensation heat transfer process of alkali metal in AMTEC porous wick condenser. The steady-state physical fields of working medium were obtained and the impacts of some relevant parameters including geometrical and operational parameters on condensation heat transfer characteristics were discussed. The results show that the thickness of the liquid sodium increases along the radial direction. The temperature distribution in liquid phase is approximately linear. The condensation rate at the phase-change interface decreases along the radial direction, and the cold end heat flux  $q$  increases initially and then decreases along the radial direction. The porous wick condenser has very limited self-adaptive ability once the mass flow rate  $M_{in}$  exceeds some critical value. In addition, there is a corresponding  $T_w$  for a certain  $M_{in}$  to ensure the stable phase-change interface. The performance of AMTEC can be enhanced by reducing the distance between artery and cell wall.*

Key words: AMTEC, porous wick condenser, condensation heat transfer, numerical simulation

## 1. Introduction

The alkali metal thermal to electric converter (AMTEC), as its name suggests, is a thermally regenerative, electrochemical device for the direct conversion of heat to electrical power using alkali metal as working medium. In recent years, AMTEC has attracted much concern due to its unique advantages such as relatively high conversion efficiency (20-30%), simple configuration, no noise and good adaptability to a variety of heat sources including nuclear energy, solar energy, heat of combustion, etc. [1, 2]. A perspective view in partial cross-section of AMTEC cell using sodium as working media is given in Fig.1 [3]. The AMTEC cell is based on an ionic selective membrane, i.e.,  $\beta''$ -alumina solid electrolyte (BASE), which only allows the sodium ions to pass through. The working principle can be described briefly as: the liquid sodium in capillary evaporator is heated by the heat

input from an external source at the hot end and becomes high-pressure sodium vapor. Then, the vapor is delivered to the BASE/anode interface where ionization of sodium metal occurs because of the thermodynamic potential across the BASE ( $Na \rightarrow e + Na^+$ ). Only the sodium ions can diffuse through the BASE to the cathode, the electrons circulate through the external load producing electrical work and then reach the cathode surface where they recombine with the sodium ions to reform sodium atoms at the BASE/cathode interface ( $Na^+ + e \rightarrow Na$ ). The sodium, in vapor form, passes through the low pressure cavity and reaches the condenser surface, where it gives up the latent heat of condensation to become liquid, and then recycle to the liquid-return artery by capillary action of the evaporator [2].

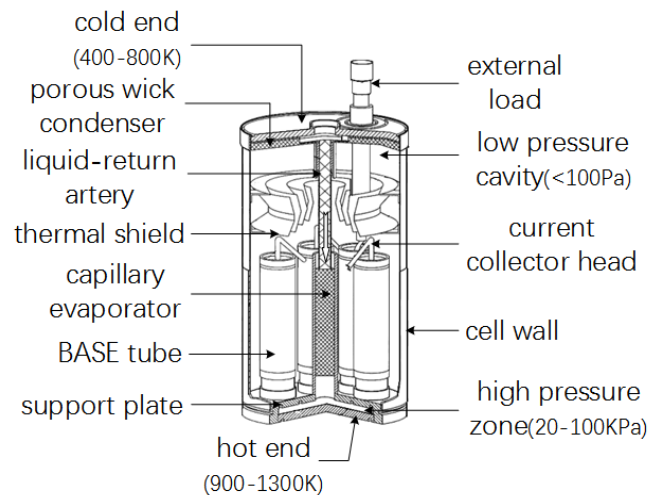


**Fig.1 A perspective view in partial cross-section of AMTEC cell [3]**

The authors once did a thorough review of the state of the art in the research and development of the AMTEC [2]. It was revealed that, the researches about AMTEC mainly focus on its overall performance test and optimization [4, 5], application fields [6], material and structure design [7, 8], numerical simulation of flow and thermal performance, heat loss, as well as the heat and mass transfer characteristics of capillary evaporator [9, 10]. Comparatively speaking, little attention has paid to the porous wick condenser. In fact, the porous wick condenser, which controls the circulation flow of working medium and the heat transfer inside the AMTEC, is equally important as the evaporator. On the other hand, since the heat-rejection temperature of AMTEC namely the operation temperature of condenser is 400-800K, it is cost-efficient to utilize the heat from the AMTEC condenser. If the rejected heat from the condenser is recycled, it not only can improve the overall conversion efficiency, but also can avoid thermal pollution to the environment. However, little effort has been poured into how to utilize the rejected heat of AMTEC condenser, and only a conceptual design of cascading AMTEC/TEC system has been proposed [6, 11]. As an exploratory study, the authors have proposed a parabolic dish/AMTEC solar thermal power system and evaluated its overall thermal-electric conversion performance. It should be noted that, the evaluation results were obtained on the basis of the existing empirical or semiempirical correlations. In other words, the internal heat transfer characteristics of AMTEC components including the condenser were not fully considered. Nevertheless, for a cascading system comprised of AMTEC and other heat utilization device, the heat rejection from AMTEC condenser is actually the heat source of other heat utilization device. Thus, it is necessary to research into the sodium vapor condensation heat transfer in AMTEC porous wick condenser, so as to provide guidance for the optimization of coupling conditions.

According to our analysis, for the AMTEC condenser, the sodium vapor condensates in the porous wick condenser which essentially belongs to condensation problem in porous media. Currently, the work on the condensation problem in porous medium, according to the surface geometry can be classified as vertical plate [12], horizontal plate [13], disc [14], circular tube [15], elliptical tube [16], etc. Whereas, the AMTEC wick condenser is circular ring structure, which differs from the existing research. In view of this, this article takes the AMTEC wick condenser as research subject, and establishes a physical and mathematical model to investigate the condensation heat transfer characteristics of sodium in AMTEC porous wick condenser numerically. One should notice that, the present paper emphasizes the detail research of an AMTEC component namely the porous wick condenser, which has never been reported in the existing work. The motivation behind our work is to provide theoretical guidance for the design, operation, optimization and evaluation of AMTEC itself or AMTEC cascading with other heat utilization device.

## 2. The physical and mathematical model

### 2.1. Physical model

The sketch diagram of AMTEC porous wick condenser is shown in Fig.2, a layer of porous wick such as mesh pad is arranged at the cold end internal surface. Considering the symmetry of the condenser, an axisymmetric two-dimensional model, which consists of porous wick and a part of low pressure cavity, is established in the cylindrical coordinate as shown in Fig.3. Both the low pressure cavity(F-G) and the porous wick(C-F) are 10mm in axial length, while the distance between artery and cold end ( $L_{cd}$ ) is 5mm. The radiuses of liquid-return artery and AMTEC cell are 2mm(D-E) and 17mm(B-C), respectively. The porous wick is made of Titanium whose properties are porosity  $\varepsilon=0.4$ , effective aperture  $r_p=2\times 10^{-5}$ mm, permeability  $K=4.55\times 10^{-12}$ m<sup>2</sup>.

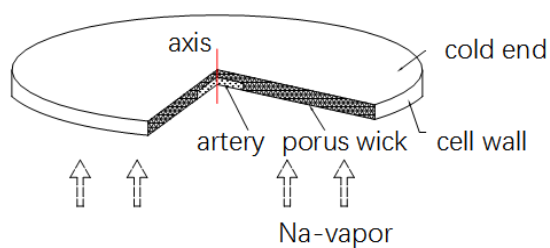


**Fig.2 Sketch diagram of AMTEC porous wick condenser**

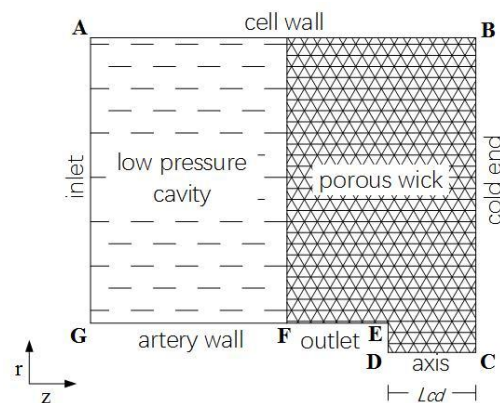


**Fig.3 Physical model of AMTEC porous wick condenser**

### 2.2. Mathematical model

The volume of fluid model (VOF) has been widely used to solve the problems involving free interface capturing and phase change heat transfer in microscale channels [17, 18]. As a

consequence, in our study, the VOF model is adopted to investigate the condensation heat transfer of sodium vapor in AMTEC porous wick condenser. Some hypotheses are employed in mathematical modeling as follows.

- 1) The porous media is homogeneous and isotropic, and meets the local thermal equilibrium assumption, namely the temperature of solid skeleton and fluid is equal.
- 2) There is no temperature difference between liquid and vapor in phase change interface, namely, the liquid membrane temperature is equal to the saturated steam temperature.
- 3) The physical properties of liquid film and porous media are constant within the range of operating temperature.
- 4) The flow is laminar in all regions, ignoring the effects of gravity and capillary force.

Continuity equation:

$$\frac{\partial}{\partial t}(\varepsilon\rho_f) + \nabla\mathbf{g}(\rho_f\mathbf{V}) = 0 \quad (1)$$

Momentum equation:

$$\frac{\rho_f}{\varepsilon} \frac{\partial \mathbf{V}}{\partial t} + \frac{\rho_f}{\varepsilon^2} (\mathbf{V}\mathbf{g}\nabla) \mathbf{V} = -\nabla P - D \frac{\mu}{K} \mathbf{V} + \frac{\mu}{\varepsilon} \nabla^2 \mathbf{V} \quad (2)$$

where  $D$  is a variable differentiating the low pressure cavity ( $D=0$ ) and the porous wick ( $D=1$ ) zone.

Energy equation:

$$\overline{\rho c} \frac{\partial T}{\partial t} + \rho_f c_f (\mathbf{V}\mathbf{g}\nabla) T = \nabla\mathbf{g}(\lambda_{\text{eff}}\nabla T) + S_h \quad (3)$$

In VOF model, tracking of the interface between the phases is accomplished by the solution of the continuity equation for the volume fraction of the secondary phase. In present paper, the liquid and vapor are set as the primary and secondary phases respectively [19], thus the VOF equation is written as.

$$\frac{\partial \alpha_v}{\partial t} + \nabla\mathbf{g}(\alpha_v\mathbf{V}) = -\frac{\dot{m}}{\rho_v} \quad (4)$$

Where  $\dot{m}$  is the mass production rate due to condensation and  $\alpha_v$  is the volume fraction factor of the vapor. If  $\alpha_v=1$ , the region is occupied by pure vapor, while if  $\alpha_v=0$  the region is pure liquid. The value of  $\alpha_v$  varies between 0 and 1, and the volume fraction of liquid is defined as  $\alpha_l=1-\alpha_v$ .

The properties in the equations above are given as the volume-fraction-averaged form, which can be written as:

$$\rho_f = \alpha_v\rho_v + (1-\alpha_v)\rho_l \quad (5)$$

$$\mu = \alpha_v\mu_v + (1-\alpha_v)\mu_l \quad (6)$$

$$\lambda_{\text{eff}} = [\alpha_v\lambda_v + (1-\alpha_v)\lambda_l]\varepsilon + (1-\varepsilon)\lambda_s \quad (7)$$

$$\overline{\rho c} = [\alpha_v\rho_v c_v + (1-\alpha_v)\rho_l c_l]\varepsilon + (1-\varepsilon)\rho_s c_s \quad (8)$$

$$c_f = [\alpha_v c_v + (1 - \alpha_v) c_l] / \rho_f \quad (9)$$

Phase change model:

The key to simulate the condensation process is the determination of the condensation rate and the latent heat transfer, which is usually achieved by adding the source terms in the governing equation. In view of the numerical implementation and convergence, Lee model, based on the kinetic gas theory, is adopted to describe the source terms in this paper [19]. Mass and energy source terms can be written as follows:

$$\dot{m} = -\beta \alpha_l \rho_l \frac{T - T_{\text{sat}}}{T_{\text{sat}}} \quad (T \geq T_{\text{sat}}) \quad (10)$$

$$\dot{m} = \beta \alpha_v \rho_v \frac{T_{\text{sat}} - T}{T_{\text{sat}}} \quad (T < T_{\text{sat}}) \quad (11)$$

$$S_h = \dot{m} h_{\text{fg}} \quad (12)$$

Where  $T$  is the local temperature of discrete control volume,  $\beta$  is mass transfer intensity factor ( $\text{s}^{-1}$ ), an excessively large  $\beta$  causes numerical convergence problem, while a too small value leads to a significant deviation between the interfacial temperature and the saturation temperature. Researchers have used a very wide range of  $\beta$  value, for instance, Yang et al. [20] performed VOF simulation of boiling in a coiled tube using the value  $\beta=100 \text{ s}^{-1}$ . Liu et al. [19] analyzed the film condensation between vertical parallel plates using VOF model, in which  $\beta$  is set as  $5000 \text{ s}^{-1}$ . Da Riva and Del Col [21] even set  $\beta$  as  $1.0 \times 10^7 \text{ s}^{-1}$  for a high mass velocity of  $G=800 \text{ kg} \cdot \text{m}^{-2} \cdot \text{s}^{-1}$ . These values were found by a trial-and-error procedure to numerically maintain the interface temperature close to saturation temperature. The coefficient  $\beta$  is set as  $6 \times 10^6 \text{ s}^{-1}$  in present work.

Boundary condition:

A-G (inlet):

$$T = T_{\text{sat}}, M = M_{\text{in}}, \alpha_v = 1 \quad (13)$$

D-E (outlet):

$$P = P_{\text{out}}, \partial T / \partial z = 0, \partial \alpha_v / \partial z = 0 \quad (14)$$

B-C (cold end):

$$T = T_w, V = 0 \quad (15)$$

C-D (axis):

$$\partial P / \partial r = 0, \partial T / \partial r = 0 \quad (16)$$

A-B (cell wall), E-G (artery wall):

$$\partial T / \partial r = 0 \quad (17)$$

The governing equations were numerically solved by finite volume method, using the commercial CFD package ANSYS FLUENT 15.0. User Defined Functions (UDF) codes were built based on Lee model to simulate the condensation process. Considering the dynamic behavior of the two-phase flow, transient calculations were carried out with a time step of  $1 \times 10^{-6}$ s for all cases. The time step was selected based on the Courant number, which is the ratio of the time step to the time a fluid takes to move across a cell. For the time step of  $1 \times 10^{-6}$ s, the Courant number is less than 0.1 which ensures the stability of the calculation. PISO (pressure-implicit with splitting of operators) algorithm is applied to the pressure and velocity coupling solution. PRESTO! (pressure staggering option) scheme was used for pressure discretization while the second order upwind scheme is employed to the momentum and energy equation. Besides, Geo-Reconstruct scheme was recommended to the volume fraction discretization. When the mass flow rate of inlet and outlet is equal, and other physical fields do not change over time, the condenser is considered in steady state operation. The physical properties of sodium and porous wick can be found in Ref [22].

### 2.3. Grid independent test and model validation

Structured grid has been adopted to the meshing process, and a local mesh refined method is used for the region where the condensation probably occurs, so as to capture the phase change interface more accurately. In order to test the grid dependency on the model, three groups of grid number are considered. As shown in Table 1, the minimum film thickness ( $\delta_{\min}$ ) and the average temperatures of outlet ( $T_{\text{out}}$ ) are monitored, taking a typical working condition, i.e.,  $M_{\text{in}}=3\text{mg/s}$ ,  $T_{\text{sat}}=650\text{K}$ ,  $T_{\text{w}}=646\text{K}$  as example. To balance the accuracy and arithmetic speed, the total grid number of 108900 is chosen to solve the mathematical equations.

**Table 1 Grid independency test**

Grid number	98000	108900	122800
$\delta_{\min}/\text{mm}$	9.76	9.78	9.78
$T_{\text{out}}/\text{K}$	647.11	647.10	647.10

To verify the reliability of the current model in solving the condensation problem in porous media, a plat type condenser with porous wick using methyl alcohol as working fluid was calculated. Geometric dimensions and operating parameters of the condenser are the same as those in the Ref [23]. Comparing the distributions of vapor phase volume fraction and temperature shown in Fig. 4, the results of the present model agree well with those in Ref [23] and the Geo-Reconstruct scheme used in this paper effectively avoids fuzzy interface. Qu et al. [24] conducted a visual experimental research on the same plat type condenser with porous wick, and the shape of the liquid film at steady state is given in Fig.5. The black area represents the liquid phase, while the white area represents the vapor phase. In the visualization experiment, the velocity of the inlet is 0.6m/s and the temperature of the inlet is 337.15K. The temperature difference between the inlet and cold wall is set to be 10K. It is observed that interfaces of present model and Qu et al show similar shape. Hence, the calculation model provided in this paper can be used with confidence.

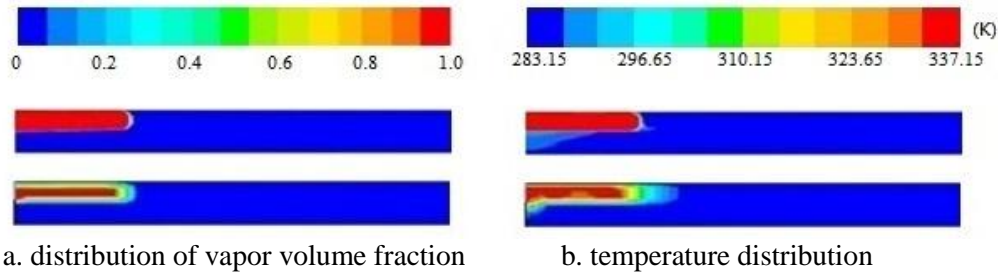


**Fig.4 Results comparison between present work (*top*) and Ref [23] (*bottom*)**



**Fig.5 Visualization experimental result of Qu et al. [24]**

### 3. Results and discussion

#### 3.1. Physical fields in porous wick condenser

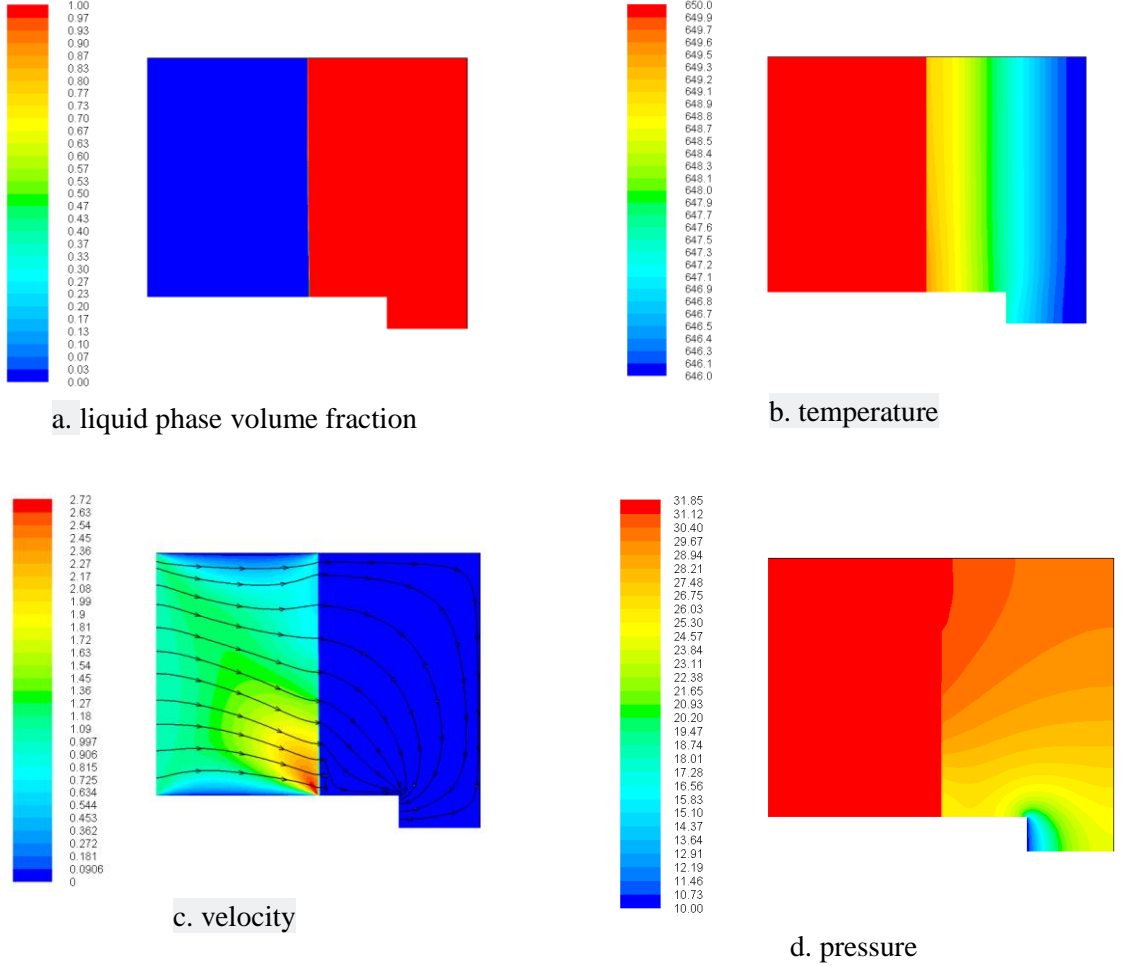
The steady-state distributions of liquid phase volume fraction, temperature, velocity and pressure of working medium were obtained under the condition of  $M_{in}=3\text{mg/s}$ ,  $T_{sat}=650\text{K}$ ,  $T_w=646\text{K}$  as shown in Fig.6. Initially, the porous wick zone is filled with liquid sodium, while the low pressure cavity is full of saturated sodium vapor.

The distribution of liquid phase volume fraction is given in Fig.6a, where the blue and red regions represent the sodium vapor and liquid respectively. It can be found that a stable vapor-liquid interface is maintained nearby the surface of the porous wick, that is to say, all sodium vapor starts to condensate once enter the porous wick region. It should be noted that the thickness of the sodium liquid film  $\delta$  increases continuously along the radial direction  $r$  as shown Fig.7(left); however, the range of this variation is less than 0.2mm, thus the porous wick condenser shown in Fig.6a seems like to be filled with liquid sodium with the naked eye. Moreover, the liquid-vapor two phase region is extremely thin which agree with Shi's [25] conclusion that thickness of the transition region from vapor to liquid is very thin, only about 1-2 molecular diameter.

Fig.6b shows the distribution of the temperature. Clearly, temperature in vapor phase is constant, while the temperature distribution in the liquid phase is linear approximately. The reasons can be explained as follows. In low pressure cavity, the temperatures of the inlet vapor and the phase change interface are both assumed to equal to the saturated steam temperature  $T_{sat}$ , thus there is no temperature gradient. As for the porous wick region, the effective thermal conductivity  $\lambda_{eff}$  is large enough ( $\lambda_{eff}=46.7 \text{ W}\cdot\text{m}^{-1}\cdot\text{K}^{-1}$ ), on the other hand, the velocity of liquid sodium after condensation is extremely small (in the order of  $10^{-5}\text{m/s}$ ), as shown in Fig.6c. Hence, the latent heat releases mainly through heat conduction, the influence of convection is negligible, so that the temperature is linearly distributed along the axial direction.

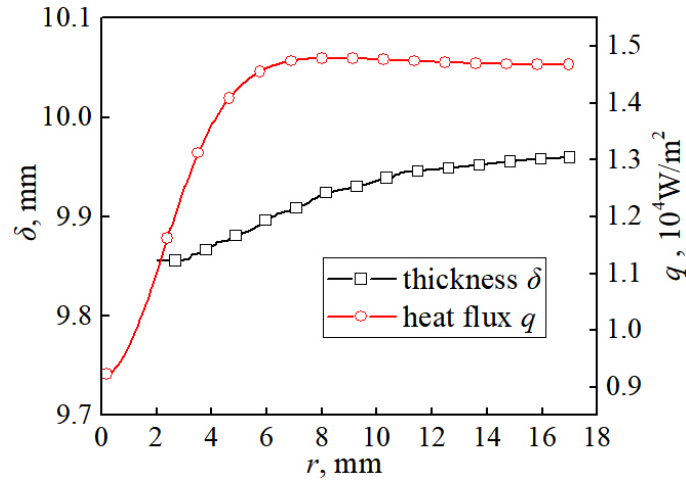
The velocity contour combined with the pathline is shown in Fig.6c. It can be found that the velocity of the sodium vapor increases significantly at the porous wick surface near the liquid-return artery; whereas, the velocity decreases at the porous wick surface near the cell wall. According to the

pathline, the sodium vapor tend to flow towards the region around the liquid-return artery. The facts above mean that the mass flow rate of the sodium vapor flow is not evenly distributed but decreases along the radial direction. Consequently, a similar trend is presented in the distribution of cold end heat flux  $q$  as shown in Fig.7(right). However, it should be noted that the cold end heat flux increases initially ( $0 < r < 7$ , mm) and then decreases ( $7 < r < 17$ , mm) along the radial direction rather than monotone decreasing. This trend is mainly due to the fact that the heat transfer area between the outlet and the cold end gets increased which reduces the local heat flux; moreover, all the cooling sodium liquid eventually converges to the outlet causing a lower temperature near the outlet. In addition, under a steady-state operation condition the heat released from the cold end should be equal to the condensation latent heat based on theoretical analysis. When the mass flow rate of inlet  $M_{in}$  is 3mg/s, the total heat transfer rate  $Q$  should be 13.2W. Integrating the cold end heat flux along radial direction, the total heat transfer rate  $Q'$  is calculated to be 12.9W, namely  $Q \approx Q'$  which further illustrates the rationality of the present model.



**Fig.6 Contours of phase, temperature, velocity and pressure**





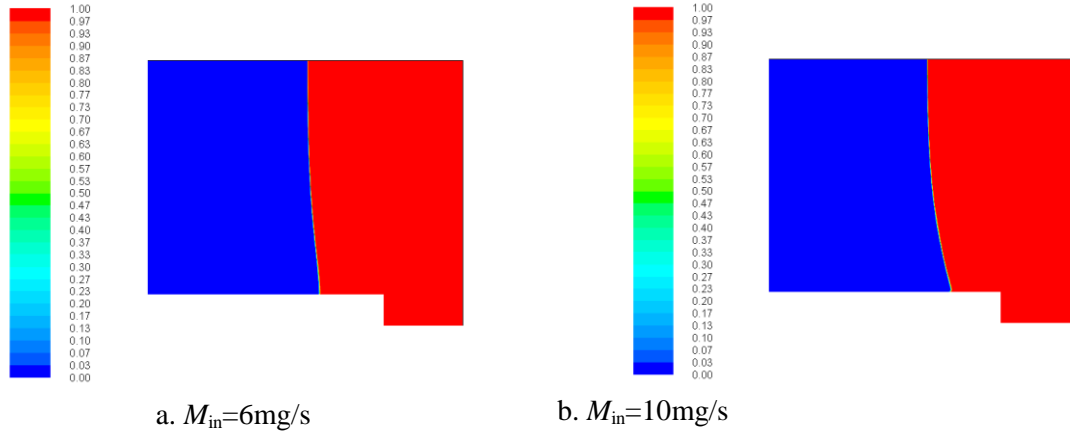
**Fig.7 Distribution of  $\delta$  (left) and  $q$  (right) along the radial direction**

Fig.6d shows the contour of pressure, usually, the pressure in the low pressure cavity is less than 100Pa. The effect of the heat shield of AMTEC is not considered, so that the flow resistance in low pressure cavity is very small and the pressure of vapor phase is almost unchanged. Because of the assumption that the flow is laminar, the influence of inertia resistance is ignored, the flow resistance in the porous wick is only derived from the viscous stress. In the region around the liquid-return artery, the flow resistance is much smaller, thus more sodium vapor tends to condensate at the surface nearby liquid-return artery.

### 3.2. The effect of mass flow rate

In actual operation, the mass flow rate of an AMTEC tends to fluctuate with the hot end heat input. The more heat is supplied to the hot end, the greater the amount of sodium vapor flowing out of the capillary evaporator. Consequently, the condenser should be self-adaptive to ensure that sodium vapor condensates completely in the porous wick, and only liquid sodium returns to the artery, otherwise the loop of the whole AMTEC may be interrupted.

The contours of phase under different mass flow rate  $M_{in}$  is shown in Fig.8, where  $T_{sat}=650\text{K}$ ,  $T_w=646\text{K}$ , and the distribution of  $\delta$  along the radial direction is given in Fig.9(left) It is obvious that the entire vapor-liquid interface moves into the porous wick as the  $M_{in}$  increases, meanwhile, the moving distance decreases along the radial direction. This suggests that the porous wick condenser can meet the requirement of steady condition by adjusting the position and shape of the interface. In this way, the heat transfer area is increased, and the decreasing thickness of liquid sodium can also reduce the heat transfer resistance, thus the condensation process is enhanced. However, this self-adaptive ability is limited. The simulation results indicate that once the mass flow rate increases to  $M_{in}=15\text{mg/s}$ , the interface front extends to the outlet, suggesting that some uncondensed sodium vapor flow into the liquid-return artery, and the condenser reaches its working limitation. Additionally, distributions of  $q$  show similar tendency under different  $M_{in}$ , i.e.,  $q$  increases initially and then decreases along the radial direction as shown in Fig9(right). However, the decreasing  $\delta$  increases the inhomogeneity of the cold end heat flux  $q$ . When  $M_{in}=10\text{mg/s}$ , the  $q$  at a small  $r$  is close to 0, and changes more sharply along the radial direction.



**Fig.8 Contours of liquid phase under different  $M_{in}$**

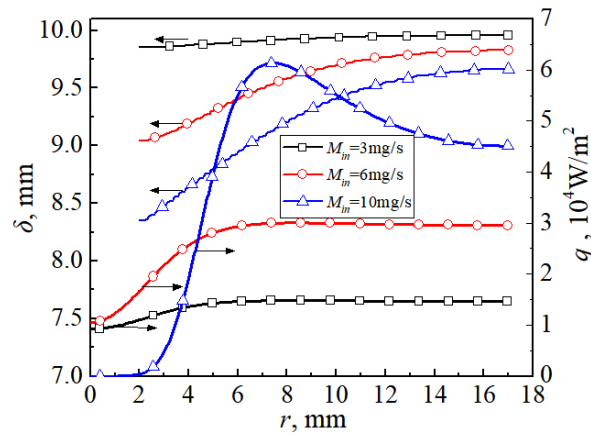


**Fig.9 Distribution of  $\delta$  (left) and  $q$  (right) along the radial direction**

### 3.3. The effect of cold wall temperature

Under an ideal working situation, the vapor-liquid in-terface is expected to stay steady on the surface of the porous wick condenser. This interface reduces radiative heat losses to the condenser because of its high reflectivity. The cold wall temperature  $T_w$  is a key parameter to determine the amount of condensation and the shape of the interface directly.

Fig.10(left) illustrates the distribution of liquid sodium thickness film along the radial direction under different  $T_w$ , when  $M_{in}=10\text{mg/s}$ . It can be found that the interface front goes deep into the porous wick when  $T_w=646\text{K}$ , the thickness of liquid sodium film  $\delta$  increases along the decreasing temperature and the lower  $T_w$  causes a smaller growth rate of  $\delta$ . When  $T_w=639\text{K}$ , the interface is close to an ideal state, the film thickness varies slightly along the radial direction, which is similar to the distribution in Fig.6a ( $M_{in}=3\text{mg/s}$ ,  $T_w=646\text{K}$ ). It means that there is a corresponding  $T_w$  for a certain  $M_{in}$  to ensure the stable vapor-liquid interface inside the porous wick condenser. Besides, the greater the mass flow rate becomes, the smaller this corresponding  $T_w$  is. It should be noted that, if the  $T_w$  continue to decrease after reaching optimal value, the sodium vapor will condensate before getting to the porous wick, thus make the pressure in the low pressure cavity fluctuate strongly. This is not allowed in the actual operation. In addition, Fig.10(right) shows the distribution of  $q$  along the radial direction, the lower  $T_w$  causes a smaller peak value and a more uniform distribution of  $q$ .

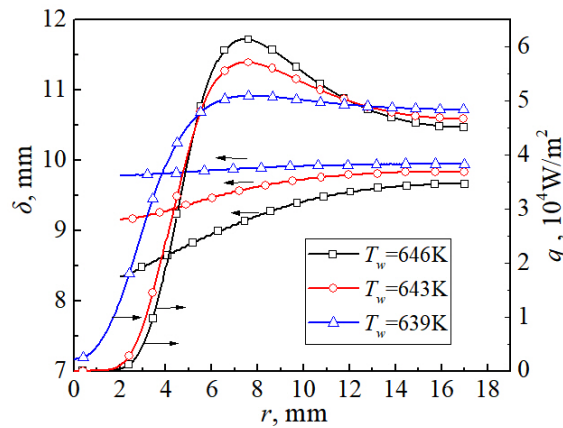


Fig.10 Distribution of  $\delta$  (left) and  $q$  (right) along the radial direction ( $M_{in}=10\text{mg/s}$ )

### 3.4. The effect of distance between artery and cold end

All the results above are obtained under the condition that the distance between artery and cell wall  $L_{cd}$  is 5mm. This section will study the effect of  $L_{cd}$  on the performance of the condenser under the operation condition that  $T_{sat}=650\text{K}$ ,  $T_w=646\text{K}$ ,  $M_{in}=3\text{mg/s}$ , and the  $L_{cd}$  is taken to be 3mm, 2mm respectively.

Fig.11 shows the contours of temperature under different  $L_{cd}$ , it can be seen that changing the distance between artery and cell wall has little effect on the temperature field in the porous wick, but it has a significant influence on the temperature distribution at the outlet compared with the Fig.6b. As shown in Fig.12, the outlet temperature increases gradually along the radial direction, and the smaller the  $L_{cd}$ , the lower the  $T_{out}$ . Actually, the  $T_{out}$  is always expected to be lower. It is due to that heat input of the hot end will heat liquid sodium in the artery, and the capillary evaporator may become dry if this heat input is too large. The lower temperature of liquid sodium can reduce the dry-out risk of evaporator. It is also shown that changing the distance has little impact on the distribution of  $\delta$  as is shown in Fig.13(left). Hence the performance of AMTEC is enhanced by a smaller  $L_{cd}$ . Besides, the distance  $L_{cd}$  also influences the distribution of cold end heat flux  $q$  as shown in Fig.13(right). Although the general distributions of  $q$  under different  $L_{cd}$  are similar, the peak value of  $q$  increases with the decreasing  $L_{cd}$ , and radial location where the maximum  $q$  appears moves to the centre as the  $L_{cd}$  reduces.

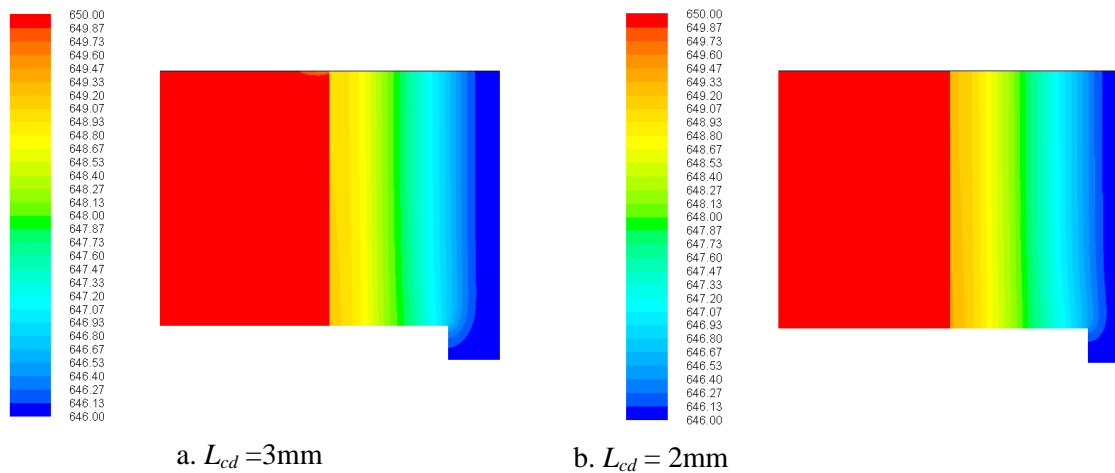
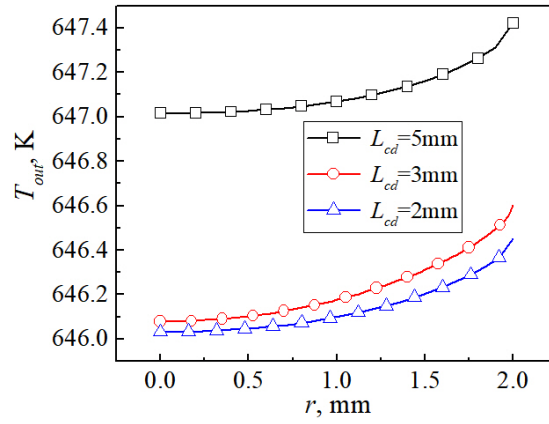
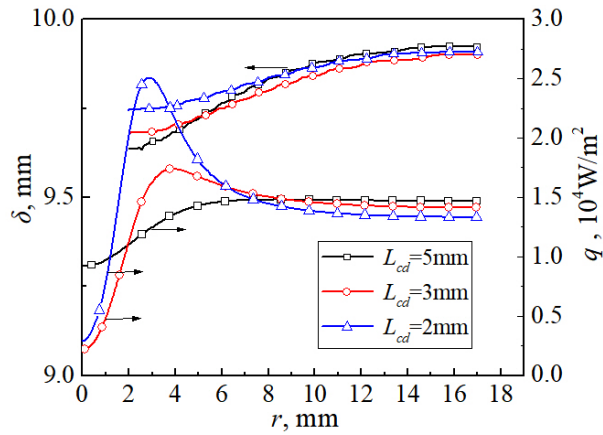


Fig.11 Contours of temperature under different  $L_{cd}$



**Fig.12 Temperature distribution at the outlet  $T_{out}$  under different  $L_{cd}$**



**Fig.13 Distribution of  $\delta$  (left) and  $q$  (right) along the radial direction**

#### 4. Conclusions

The porous wick condenser is an important component which controls the circulation, heat and mass transfer of alkali metal thermal to electric converter (AMTEC). In this paper, a physical and mathematical model for the sodium vapor condensation heat transfer of the AMTEC porous wick condenser was established. Through numerical simulation, the steady-state distributions of physical fields were obtained and the influences of the relevant parameters on the condensation heat transfer characteristics were discussed.

The results reveal that, for an ideal working situation, the thickness of liquid sodium film  $\delta$  increases gradually along the radial direction, the temperature distribution in liquid phase is approximately linear, while the temperature in vapor is constant. Moreover, the condensation rate of sodium vapor on the phase-change interface decreases along the radial direction, and the cold end heat flux increases initially and then decreases along the radial direction. The porous wick condenser has very limited self-adaptive ability once the mass flow rate  $M_{in}$  increased. In addition, there is a corresponding  $T_w$  for a certain  $M_{in}$  to ensure the stable phase-change interface in the porous wick condenser. The greater the mass flow rate becomes, the smaller the corresponding  $T_w$  is. Finally, changing the distance between artery and cell wall has significant influences on the outlet temperature and the cold end heat flux. The performance of AMTEC can be enhanced by a smaller  $L_{cd}$ .

#### Acknowledgement

This work is supported by National Natural Science Foundation of China (Project No.51306215).

## Nomenclature

$C$	heat capacity ( $\text{J}\cdot\text{kg}^{-1}\cdot\text{K}^{-1}$ )	<b>Greek symbols</b>	
$D$	variable differentiating the low pressure cavity and the porous wick	$\varepsilon$	porosity
$h_{fg}$	latent heat ( $\text{J}/\text{kg}$ )	$\alpha$	volume fraction
$K$	permeability ( $\text{m}^2$ )	$\beta$	mass transfer intensity factor
$\dot{m}$	mass production rate of condensation ( $\text{kg}\cdot\text{m}^{-3}\cdot\text{s}^{-1}$ )	$\rho$	density ( $\text{kg}/\text{m}^3$ )
$M_{in}$	mass flow at inlet ( $\text{kg}/\text{s}$ )	$\lambda$	thermal conductivity ( $\text{W}\cdot\text{m}^{-1}\cdot\text{K}^{-1}$ )
$L_{cd}$	distance between artery and cold end (mm)	$\lambda_{eff}$	effective thermal conductivity ( $\text{W}\cdot\text{m}^{-1}\cdot\text{K}^{-1}$ )
$P$	pressure (Pa)	$\mu$	viscosity ( $\text{kg}\cdot\text{m}^{-1}\cdot\text{s}^{-1}$ )
$P_{out}$	pressure at outlet (Pa)	$\delta$	thickness of liquid film (mm)
$q$	cold end heat flux ( $\text{W}/\text{m}^2$ )		
$Q$	heat transfer rate (W)	<b>Subscripts</b>	
$Q'$	calculated total heat transfer rate (W)	f	working fluid
$r$	radial coordinate (mm)	in	inlet
$r_p$	effective aperture (m)	l	liquid phase
$S_h$	energy source term ( $\text{J}\cdot\text{m}^{-3}\cdot\text{s}^{-1}$ )	out	outlet
$t$	time (s)	s	solid phase
$T$	temperature (K)	sat	saturation state
$T_{sat}$	saturation temperature (K)	v	vapor phase
$V$	superficial velocity (m/s)	w	wall
$z$	axial coordinate (mm)		

## References

- [1] Lodhi, M.A.K., *et al.*, An Overview of Advanced Space/Terrestrial Power Generation Device: AMTEC, *Journal of Power Sources*, 103(2001), 1, pp. 25-33
- [2] Wu, S.Y., *et al.*, A Review on Advances in Alkali Metal Thermal to Electric Converters (AMTECs), *International Journal of Energy Research*, 33(2009), 10, pp. 868-892
- [3] Svedberg, R.C., *et al.*, Heat Shields for Alkali Metal Thermal to Electric Conversion (AMTEC) Cells, *United State Patent*, 1999
- [4] Tournier, J., El-Genk, M.S., Performance Analysis of Pluto/Express, Multitube AMTEC Cells, *Energy Conversion & Management*, 40(1999), 2, pp. 139-173
- [5] Tournier, J.M., *et al.*, AMTEC Performance and Evaluation Analysis Model (APEAM): Comparison with Test Results of PX-4C, PX-5a, and PX-3a Cells, *AIP Conference Proceedings*, 420(1998), 1, pp. 1576-1585
- [6] El-Genk, M.S., Tournier, J.M.P., Analyses of Static Energy Conversion Systems for Small Nuclear Power Plants, *Progress in Nuclear Energy*, 42(2003), 3, pp. 283-310

- [7] El-Genk, M.S., Tournier, J.M., Performance Comparison of Potassium and Sodium Vapor Anode, Multi-Tube Amtec Converters, *Energy Conversion & Management*, 43(2002), 15, pp. 1931-1951
- [8] Lodhi, M.A.K., Daloglu, A., Performance Parameters of Material Studies for AMTEC Cell, *Journal of Power Sources*, 85(2000), 2, pp. 203-211
- [9] Wu, S.Y., *et al.*, Influence of Working Fluids and Wick Materials on Performance of Porous Wick Evaporator Based on AMTEC, *Journal of Engineering Thermophysics*, 33(2012), 12, pp. 2150
- [10] Wu, S.Y., *et al.*, Parametric Study on Flow and Heat Transfer Characteristics of Porous Wick Evaporator Based on AMTEC, *Journal of Mechanical Science and Technology*, 26(2012), 3, pp. 973-981
- [11] El-Genk, M.S., King, J.C., Performance Analyses of an Nb-1Zr/C-103 Vapor Anode Multi-Tube Alkali-Metal Thermal-to-Electric Conversion Cell, *Energy Conversion & Management*, 42(2001), 6, pp. 721-739
- [12] Mohamed, E.M., Rashed, A., Film Condensation Generated by Free Convection in a Porous Medium, *Thermal Science*, 2016, DOI: 10.2298/TSCII60820316M
- [13] Wang, S.C., *et al.*, Steady Filmwise Condensation with Suction on a Finite-Size Horizontal Flat Plate Embedded in a Porous Medium Based on Brinkman and Darcy Models, *International Journal of Thermal Sciences*, 45(2006), 4, pp. 367-377
- [14] Chang, T.B., Laminar Filmwise Condensation on Horizontal Disk Embedded in Porous Medium with Suction at Wall, *Journal of Heat Transfer*, 130(2008), 7, pp. 351-358
- [15] Annamalai, A.S., Ramalingam, V., Experimental Investigation and Computational Fluid Dynamics Analysis of an Air Cooled Condenser Heat Pipe, *Thermal Science*, 15(2011), 3, pp. 759-772
- [16] Chang, T.B., Yeh, W.Y., Theoretical Investigation into Condensation Heat Transfer on Horizontal Elliptical Tube in Stationary Saturated Vapor with Wall Suction, *Applied Thermal Engineering*, 31(2011), 5, pp. 946-953
- [17] Alizadehdakhel, A., *et al.*, CFD Modeling of Flow and Heat Transfer in a Thermosyphon, *International Communications in Heat and Mass Transfer*, 37(2010), 3, pp. 312-318
- [18] Zhang, Y., *et al.*, Capillary Blocking in Forced Convective Condensation in Horizontal Miniature Channels, *Journal of Heat Transfer*, 123(2001), 3, pp. 501
- [19] Liu, Z., *et al.*, VOF Modeling and Analysis of Filmwise Condensation Between Vertical Parallel Plates, *Heat Transfer Research*, 43(2012), 1, pp. 47-68
- [20] Yang, Z., *et al.*, Numerical and Experimental Investigation of Two Phase Flow During Boiling in a Coiled Tube, *International Journal of Heat & Mass Transfer*, 51(2008), 5, pp. 1003-1016
- [21] Riva, E.D., Col, D.D., Effect of Gravity During Condensation of R134a in a Circular Minichannel, *Microgravity Science and Technology*, 23(2011), 1, pp. 87-97
- [22] Zhang, H., *et al.*, *Heat Pipe Energy-saving Technology(in Chinese language)*, Chemical Industry Press, Beijing, China, 2009
- [23] Liu, Z.C., *et al.*, Numerical Simulation of Two Phase Flow and Heat Transfer in CPL Condenser with Porous Element, *Journal of Engineering Thermophysics*, 28(2007), 2, pp. 81-84
- [24] Qu, Y., *Flow and Heat Transfer Characteristics in the Porous Wick Condenser of CPL(in Chinese luaguage)*, Beijing: Tsinghua university, China, 2000
- [25] Shi, M.H., *et al.*, *Boiling and Condensation(in Chinese language)*, Higher Education Press, Beijing, China, 1995